Propagation of a randomized 600-ps laser beam in a helium gas jet over long scale lengths

J. Faure, V. Malka, and F. Amiranoff
Laboratoire pour l'Utilisation des Lasers Intenses, UMR 7605, CNRS-CEA-Ecole Polytechnique–Université Pierre et Marie Curie, 91128 Palaiseau Cedex, France

(Received 20 March 2001; published 18 July 2001)

The propagation and interaction of a randomized 600-ps laser with a helium gas jet were studied experimentally for laser intensities of 10^{14} W/cm^2. Such a study is of interest for the indirectly driven inertial confinement fusion scheme, where a randomized laser beam propagates into a gas-filled cavity over a distance of a few millimeters. The dynamics of ionization was studied using time resolved interferometry. Maps of electronic density $n_e(z,t)$ were retrieved from time resolved interferograms. The plasma temperature was studied using Thomson scattering. The results show that the laser diffracts while propagating, leading to a decrease in laser intensity and causing ionization to occur later in time. An ionization front, moving at a velocity of about $v_f \simeq 2.8\times 10^6$ m/s, was observed. Beam diffraction also causes a nonhomogeneous heating of the plasma: the entrance of the plasma is hotter than the exit. A one-dimensional model was used to fit the results. It takes into account collisional ionization and heating by inverse bremsstrahlung. The model shows very good agreement with the experiment.

DOI: 10.1103/PhysRevE.64.026404 PACS number(s): 52.38.−r, 52.35.Fp, 52.50.Jm, 52.70.−m

I. INTRODUCTION

Efficient coupling of laser energy to the target is an essential point in inertial confinement fusion (ICF). Optical smoothing techniques [1,2] are used in order to improve the uniformity of the irradiation and to enhance the coupling to the target. In the case of the indirect drive scheme [3], the laser does not interact directly with the target but interacts first with the walls of a cavity where the laser energy is converted into x rays. Before reaching the walls, the laser has to propagate through a few millimeters of gas (typically 5 mm to 1 cm of helium with an atomic density of $n_a \simeq 10^{19}$ cm^{-3}). To our knowledge, this aspect of the interaction has never been studied experimentally and this is what inspired this paper.

This paper deals with an experimental study of the propagation of a randomized 600-ps laser pulse in a helium gas jet. In real world fusion experiments, the geometry of the cavity is impractical for diagnosing what happens inside the cavity and it is difficult to distinguish the interaction with the gas from the interaction with the walls. By using a gas jet, one can concentrate on the problem of propagation in the gas and ignore other phenomena that take place during the interaction.

Our gas jets are well characterized [4] and supersonic nozzles provide a homogeneous and flat density profile, similar to the uniform gas density inside a *Hohlraum*. Using time resolved interferometry, we were able to measure ionization dynamics and to retrieve a map of the density along the laser propagation. While propagating in the gas, no ponderomotive self-focusing was observed and beam diffraction was found to be similar to vacuum diffraction: after 4 mm, we estimated the intensity to be reduced by a factor of 20. This caused ionization to start later in time as the laser propagated. Sometimes, the end of the gas jet would not even be ionized. Similarly, this implies that plasma heating is different along propagation: the electron temperature T_e is hot (up to 200 eV) at the entrance of the plasma where the laser intensity is high and cold at the exit of the plasma where the laser intensity is low.

The paper is organized as follows. Section II presents the one-dimensional (1D) model used throughout the paper for comparison with the experimental results. This model is based on the model of Denavit and Phillion [5]; it accounts for collisional ionization and laser absorption through inverse bremsstrahlung. For a better description of the experiment, a more realistic modeling of the beam diffraction for a randomized laser beam [6,7] has been added. Section III describes the experimental setup and the results. Measurements of plasma electron density and temperature are first presented and compared with the model. In addition, laser absorption measurements are presented and compared with the model in order to confirm its validity.

II. MODEL

Before entering into the details of the model, let us consider the different parameters of interest for the propagation of a randomized laser beam over long scale lengths. First, one can define an analog of the Rayleigh length for a smoothed beam [7]: $z_R \simeq k_0 r_0 \rho_0/2$, where k_0 is the wave vector, r_0 the radius of the focal spot, and ρ_0 the speckle radius. If f is the focal length of the focusing optics, λ_0 the central laser wavelength, D the diameter of the incoming beam, and h the dimension of a cell on the random phase plate (RPP), then $r_0 = \lambda_0 f/h$ and $\rho_0 = \lambda_0 f/D$. These different dimensions are represented on Fig. 1. The parameters of the experiment are $\lambda_0 = 0.53$ μm, $D = 90$ mm, $f = 250$ mm, $h = 1$ mm, giving $r_0 = 130$ μm, $\rho_0 = 1.5$ μm, and $z_R = 1.1$ mm. For a real ICF experiment, the parameters are $\lambda_0 = 0.35$ μm, $r_0 = 200$ μm, $\rho_0 = 2-10$ μm, and $z_R = 3-20$ mm. The size of the cavity is typically $L_{int} = 10$ mm, and in some cases (depending on the focusing optics) $L_{int} > z_R$.

When the interaction length L_{int} is such that $L_{int} < z_R$, it is possible to generate uniform plasmas along the propagation axis [8]. On the contrary, when $L_{int} > z_R$, as the laser

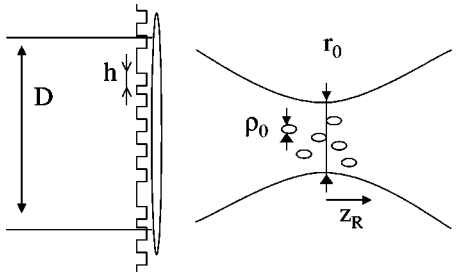

FIG. 1. Schematics of the focusing optics and different beam scales.

propagates, it diffracts and the intensity decreases along the propagation. This leads to a plasma that is not uniform (in terms of temperature and density) along the propagation axis. This is the case in our experiment and can also be the case for ICF in the indirect drive scheme. Therefore, a correct description of beam defocusing is required.

Hydrodynamic motion is to be considered when the pulse duration τ is much longer than the typical time of plasma expansion τ_{hydro}. This hydrodynamic time can be estimated as $\tau_{hydro}=r_0/c_S$, where c_S is the ion sound velocity. In our experiment, $T_e<400$ eV and $r_0>150$ μm, which gives $\tau_{hydro}>1.1$ ns$>\tau$ (600 ps). Hydrodynamic motion can therefore reasonably be neglected in our experiment.

The model [5] used in this paper simulates collisional ionization and plasma heating by inverse bremsstrahlung. It neglects hydrodynamic motion, heat conduction, and temperature equilibration with ions. Temperature equilibration with ions can reasonably be neglected because the ion temperature T_i was measured in the experiment and was found to be much smaller than the electron temperature T_e. The mechanism for ionization is as follows: The first free electrons are created through multiphoton ionization, and then collisions are responsible for ionization. The model does not include multiphoton ionization and at the beginning of each simulation the plasma is supposed to be in a low charge state. The initial number of electrons n_{e0} leads to the initial average state of the plasma $Z_{av0}=n_{e0}/n_a$ where n_a is the density of neutral atoms in the gas. The evolution of the plasma electron density n_e can be obtained by solving

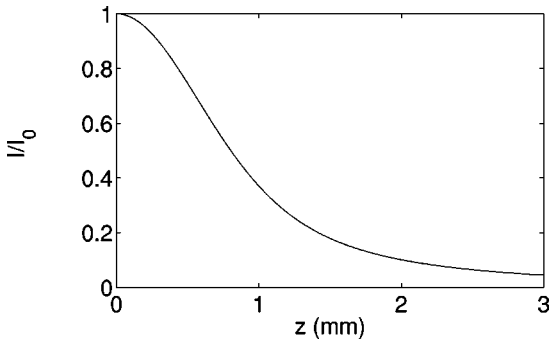

FIG. 2. Decrease of the on-axis intensity of a smoothed beam due to diffraction. Parameters are $r_0=130$ μm, $\rho_0=1.5$ μm, $z_R=1.1$ mm.

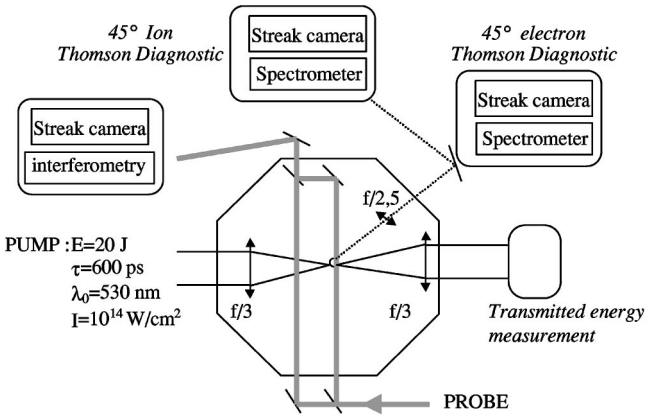

FIG. 3. Schematics of the experimental setup.

$$\frac{\partial}{\partial t}n_Z=n_e(n_{Z-1}S_Z-n_ZS_{Z+1}), \tag{1}$$

$$n_e=\sum_{Z=1}^{Z_{max}} Zn_Z, \tag{2}$$

where n_Z is the density of ions of charge Z, S_Z is the collisional ionization rate for creating ions of charge Z [9], and Z_{max} is the charge of fully stripped ions. In this description, recombination rates have been omitted, which is valid for relatively low Z elements, for temperatures lower than a few keV, and for low density plasmas. In these conditions, the recombination times are much longer than the corresponding ionization times. In the case of helium ($Z=2$), these equations are easy to solve and one can calculate the populations n_a, n_1, n_2, n_e and retrieve the average charge state of the plasma $Z_{av}=n_e/n_a$.

The temperature can be calculated using the electron energy equation

$$\frac{\partial}{\partial t}T_e=\frac{2\kappa}{3n_ak_B}\frac{I}{Z_{av}T_e^{3/2}}-\frac{T_e}{Z_{av}}\frac{\partial}{\partial t}Z_{av}-(\partial T_e/\partial t)_{ioniz} \tag{3}$$

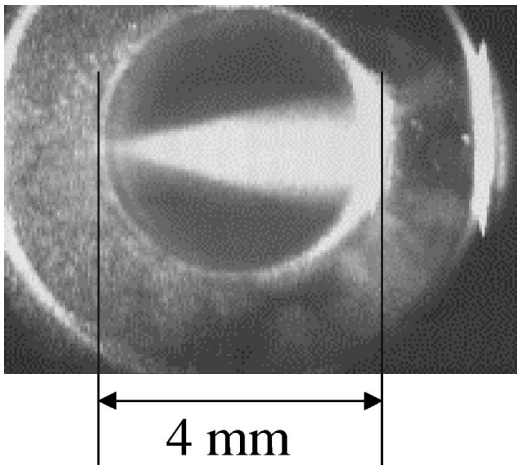

FIG. 4. Top view image of the interaction for a gas density of $n_a=1.5\times10^{19}$ cm^{-3}.

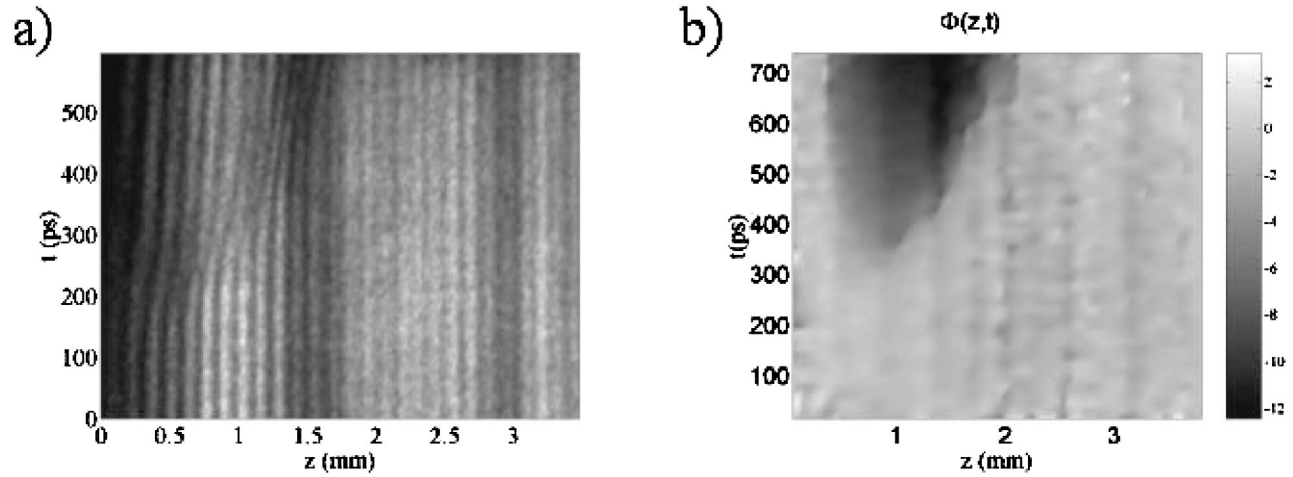

FIG. 5. (a) Interferogram for $n_a = 0.6 \times 10^{19}$ cm^{-3}. (b) Phase map $\Phi(z,t)$ obtained after analysis of the interferogram.

where Eq. (3) is in Gaussian units. The temperature T_e is in eV, $k_B = 1.6 \times 10^{-12}$ erg/eV is the Boltzmann constant, and I is the laser intensity. Finally, κ is defined as

$$\kappa = 10^{-16} Z_{av} n_e^2 / n_a \ln \Lambda \tag{4}$$

where $\ln \Lambda$ is the Coulomb logarithm calculated from Ref. [10]. The first and second terms on the right hand side of Eq. (3) represent heating by inverse bremsstrahlung in a plasma with a time varying electron density. The third term stands for the temperature loss due to ionization:

$$(\partial T_e / \partial t)_{ioniz} = \frac{2}{3} \sum_{Z=1}^{Z_{max}} n_{Z-1} S_Z \chi_Z \tag{5}$$

where χ_Z is the ionization potential for charge state Z.

When the overall intensity profile is Gaussian in the focal plane, the on-axis laser intensity in vacuum evolves as [7]

$$I^{vac}(z, r=0) = \frac{I_0}{\pi^2} \left(\frac{z_0}{z} \right)^2 (1 - e^{-\pi^2 z^2 / z_0^2}) \tag{6}$$

where $z_0 = k_0 r_0 \rho_0$. The decrease of laser intensity for the parameters of our experiment is shown in Fig. 2.

Taking into account laser absorption by inverse bremsstrahlung and diffraction effects, a differential equation for the evolution of laser intensity can then be written as

$$\frac{\partial}{\partial z} I = f(z) - \frac{\kappa I}{T_e^{3/2}} \tag{7}$$

where $f(z)$ is the derivative of Eq. (6) with respect to z.

This set of equations describes most of the physics we investigated in our experiment. Thermal conduction has been neglected, which leads to an overestimation of the temperature: this model was previously compared with an experiment [8] and was observed to give temperatures 20% higher when compared to experimental results. The validity of this model is limited to cases where hydrodynamic motion can be neglected and to low Z elements. For high Z elements, other effects such as radiative cooling can complicate the physics at stake. It should be noted that this model also fails to describe high density and/or high intensity cases since paramet-

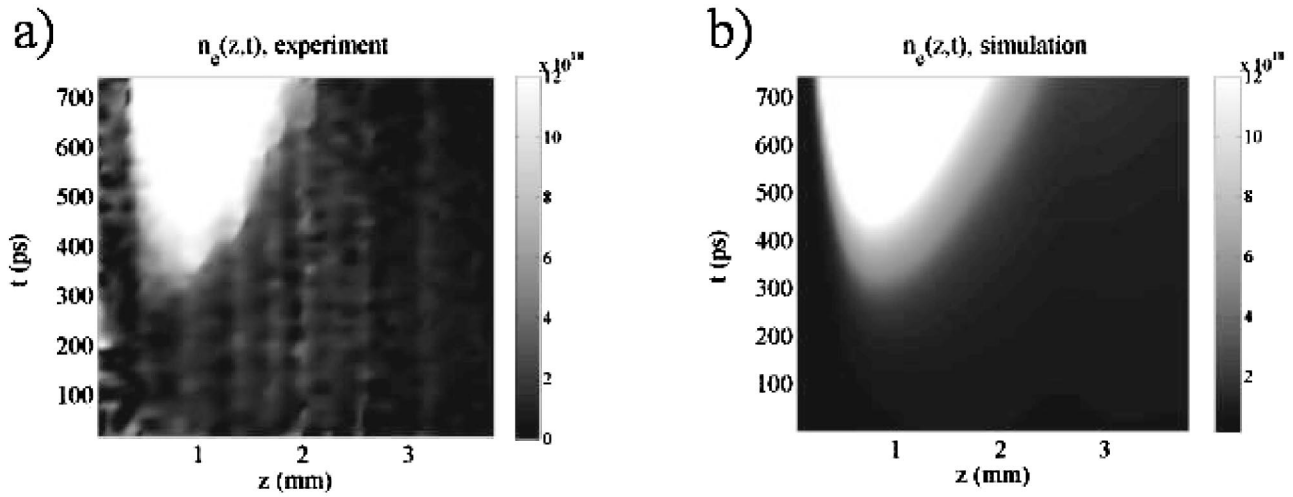

FIG. 6. (a) Experimental density map $n_e(z,t)$. (b) Simulated density map. Same parameters as Fig. 5.

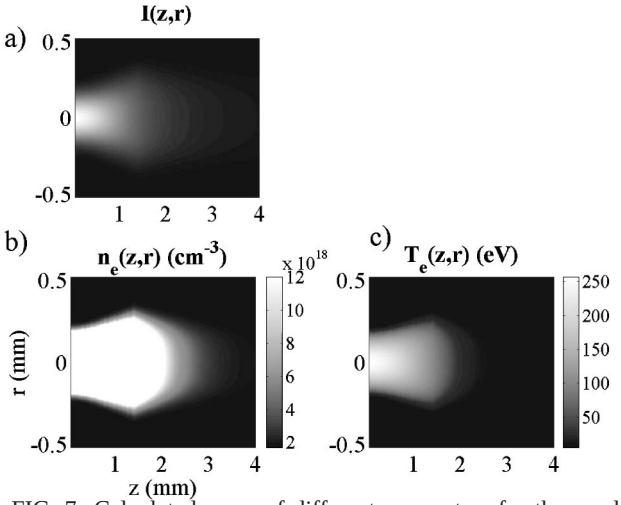

FIG. 7. Calculated maps of different parameters for the conditions of Fig. 5. (a) Intensity map $I(r,z)$. (b) Electron density map $n_e(r,z)$ at time $t=700$ ps. (c) Temperature map $T_e(r,z)$ at time $t=700$ ps.

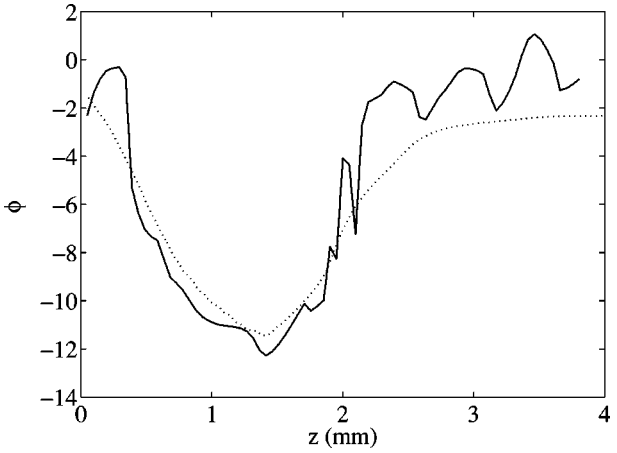

FIG. 8. Phase as a function of z at the end of the pulse (corresponding to $t=700$ ps in Fig. 6). The dotted line corresponds to the simulation and the full line to the experiment.

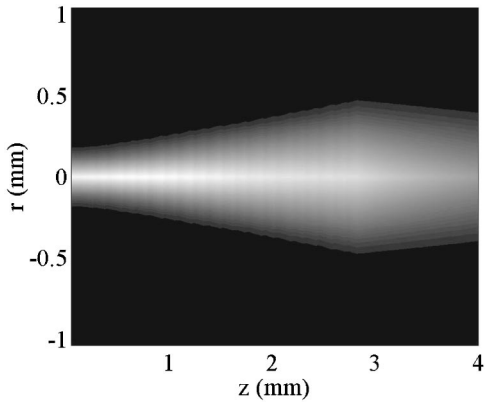

FIG. 9. Simulated top view image of the scattered light for a gas density of $n_a=1.5\times10^{19}$ cm^{-3}.

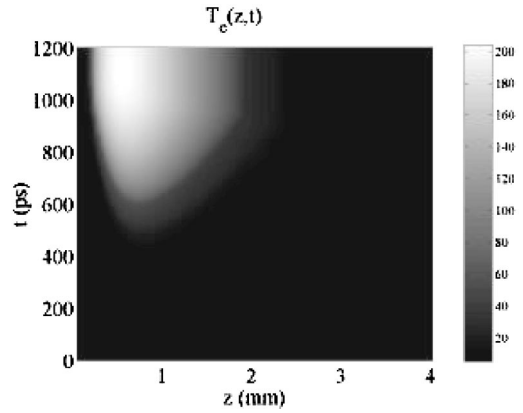

FIG. 10. Simulated map of the temperature $T_e(z,t)$. Same parameters as Fig. 5.

ric instabilities become important for dense plasmas [11] and can modify laser absorption as well as laser propagation.

Finally, using the 2D intensity distribution $I(r,z)$ calculated in Ref. [7], one can calculate the local density and temperature in 2D: respectively, $n_e(r,z)$ and $T_e(r,z)$. This is valid only if laser absorption is neglected in Eq. (7). For very underdense plasmas ($n_e<2\times10^{19}$ cm^{-3}), laser absorption was measured to be only a few percent and the laser propagation was similar to propagation in vacuum.

III. EXPERIMENT

A. Setup

The experiment was performed using one arm of the laser at the Laboratoire pour l'Utilisation des Lasers Intenses (LULI). The experimental setup is presented in Fig. 3. The infrared laser (1.054 μm) was frequency doubled (0.53 μm) using a potassium diphosphate crystal, giving a linear polarization at 45° with respect to the horizontal plane. The pulse duration of the frequency-doubled pulse was 660 ps full width at half maximum with a super-Gaussian (almost square) pulse temporal profile. The 90-mm diameter laser beam was focused on the edge of a helium gas jet with an $f/3$ doublet lens. A random phase plate with 1-mm cells was used in order to generate a large focal spot. The laser intensity distribution in the focal plane had a Gaussian enve-

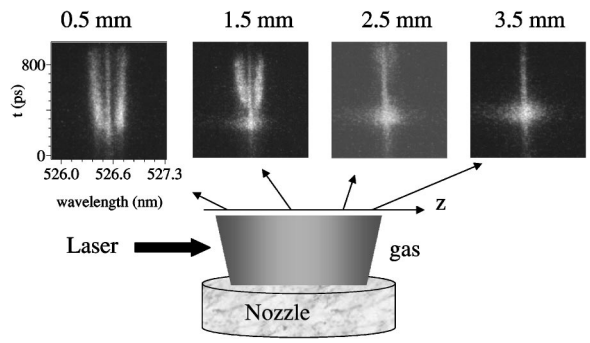

FIG. 11. Thomson spectra for different positions in the gas jet and for a density $n_a=1.5\times10^{19}$ cm^{-3}.

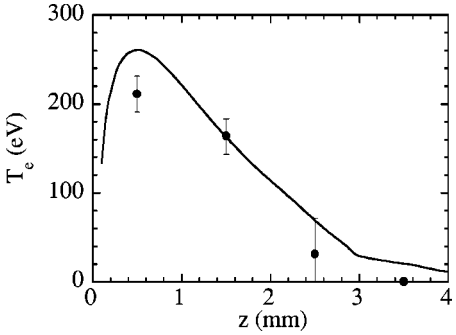

FIG. 12. Electron temperature T_e (after 300 ps) as a function of space for density $n_a = 1.5 \times 10^{19}$ cm^{-3}. The circles represent experimental points calculated from Thomson scattering spectra in Fig. 11. The line was calculated with the model.

lope with a radius at $1/e^2$ in intensity of 130 μm. The average laser intensity in vacuum was approximately 10^{14} W/cm^2.

The electron density obtained in fully ionized helium was less than 5×10^{19} cm^{-3}. The electron density could easily be modified by changing the gas backing pressure (e.g., the pressure maintained in the small reservoir chamber before the magnetic valve).

Time resolved ion Thomson scattering spectra were obtained by imaging the spectrum from a (1200 lines/mm) spectrometer onto the entrance slit of a Hadland streak camera with 200 ps/mm sweep speed. The temporal resolution of 50 ps was limited by the spectrometer and the measured spectral resolution was 0.25 Å. The resulting time resolved spectra were recorded on a 12-bit charge-coupled device (CCD). Ion Thomson scattered light was collected at 45° in the forward direction with an achromatic $f/2.5$ lens and focused at the entrance of the spectrometer.

Time resolved electron Thomson scattering spectra were measured using a lower dispersion spectrometer (100 lines/mm) giving a spectral resolution of about 30 Å. The streak camera was used with 100 ps/mm sweep speed with 10 ps time resolution. The resulting time resolved spectra were also recorded on a 12-bit CCD. Electron Thomson scattered light was collected at 45° in the forward direction with an achromatic $f/2.5$ lens and focused at the entrance of the spectrometer.

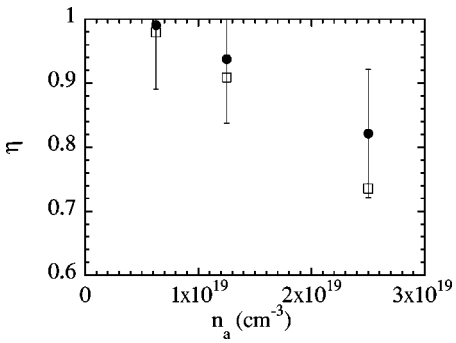

FIG. 13. Measured (circles) and calculated (squares) laser transmission as a function of gas density.

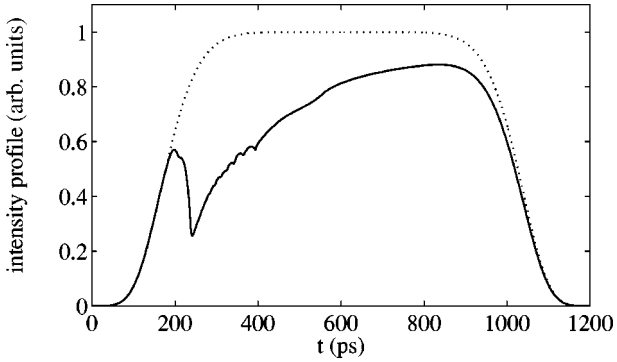

FIG. 14. Simulation of the laser intensity profile pulse before interaction (dotted line) and after interaction (full line) for a density of $n_a = 2.5 \times 10^{19}$ cm^{-3}.

Interferometry of the plasma was performed using a Mach-Zehnder interferometer. A 600-ps, frequency-doubled probe beam was used for interferometry. The probe beam was synchronized with the interaction beam and the pump-probe delay was about 100 ps (the probe was earlier). The interferogram of the plasma was imaged onto the slit of a streak camera with 100 ps/mm sweep speed. The 20-ps temporal resolution was limited by the streak camera.

A top view image of the scattered light was also set up in order to observe the beam diffraction and scattering from the plasma. Finally, laser absorption was measured by measuring the transmitted energy in an $f/3$ cone with a calibrated calorimeter. Figure 4 shows a typical top view image where one can observe the diffraction of the laser beam indicating that the Rayleigh length is shorter than the interaction length.

B. Time resolved interferometry

Time resolved interferometry gives interesting information concerning ionization dynamics along the propagation. Figure 5(a) shows a typical interferogram obtained with an initial atomic density $n_a = 0.6 \times 10^{19}$ cm^{-3}. The displacement of the fringes is indicative of ionization: the creation of electrons strongly affects the index of refraction of the medium. One might notice that the fringes start to shift later and later in time as the laser propagates: this indicates beam defocusing. Using an automatic fringe analysis program [4], it is possible to retrieve a cartography of the phase in the plane (z,t). This is what is shown in Fig. 5(b). For a low density plasma $n_e/n_c \ll 1$ (where n_c is the critical density). In this case, the phase (on axis) can be expressed as

$$\Phi(z,t) \simeq \frac{\pi}{\lambda_0} \frac{n_a}{n_c} \int_{-\infty}^{+\infty} Z_{av}(z,t,r)\,dr. \tag{8}$$

Assuming that $Z_{av}(z,t,r) = Z_{av}(z,t,r=0)$ inside the beam waist and $Z_{av} = 0$ outside, the phase reads

$$\Phi(z,t) \simeq \frac{2\pi}{\lambda_0} \frac{n_a}{n_c} Z_{av}(z,t) w(z) \tag{9}$$

where $w(z)$ is the beam radius and is defined as $w(z) = r_0 [I^{vac}(z)/I_0]^{1/2}$, with $I^{vac}(z)$ as defined in Eq. (6).

Using the phase map shown in Fig. 5(b) and Eq. (9), it is possible to retrieve an experimental electron density map $n_e(z,t)$. This is what is shown in Fig. 6(a). The simulated density map shown in Fig. 6(b) was calculated using the model described in Sec. II. The parameters for the simulation were the same as the experimental parameters: the laser pulse was 600 ps long, super-Gaussian ($I \propto \exp[-(t/\tau)^8]$) with an intensity of $I=1.5\times10^{14}$ W/cm^2, and the medium was helium at density $n_a=0.6\times10^{19}$ cm^{-3} and initially preionized so that $Z_{av0}=0.1$. The simulation reproduces the experimental results with quantitative agreement, indicating that the main reason for the delayed ionization is beam diffraction. This measurement gives information on the speed of the ionization front. For example, in Fig. 6, the ionization front moves at the velocity $v_f \simeq 2.8\times10^6$ m/s. The velocity of the front is limited by the fact that the beam diffracts and the intensity decreases: if the intensity was constant during propagation, the front velocity would be much higher and limited only by a laser absorption wave [5]. We find that, even for distances smaller than the Rayleigh length, the front velocity is limited by beam diffraction.

Bidimensional calculations were carried out as explained in Sec. II. The results are shown in Fig. 7 where the parameters in the plane (r,z) are represented at the end of the interaction. One can observe a fully ionized uniform plasma over a distance of about 2 mm. From this 2D calculation, the phase $\Phi(z,t)$ can be calculated according to Eq. (8) by integrating over the transverse coordinate. A comparison between theory and experiment is shown in Fig. 8. The dashed line is the simulated phase and it very closely reproduces the experiment (full line), indicating that beam diffraction and ionization dynamics have been described correctly. A top view image of the scattered light can also be generated using this 2D calculation. The result is shown in Fig. 9; the image is comparable to the experimental top view image in Fig. 4.

Figure 10 is a calculated temperature map $T_e(z,t)$; it illustrates that, while the temperature is about 200 eV at the entrance of the plasma (and at the end of the interaction), it falls down to about 60 eV after a 2-mm propagation. This temperature decrease can easily be explained by the fact that, when ionization occurs later in the pulse reference frame, only the back of the pulse is available for plasma heating.

Figure 11 shows Thomson scattering spectra taken at different positions along the propagation for $n_a=1.5\times10^{19}$ cm^{-3}. The spectra show that scattering occurs later as the laser pulse propagates inside the target, indicating delayed ionization. This is in agreement with our previous observation. Furthermore, the analysis of Thomson spectra shows that the temperature decreases during propagation, in agreement with the simulations. This is shown in Fig. 12: for $n_a=1.5\times10^{19}$ cm^{-3}, after 300 ps of interaction (middle of the pulse), the temperature is about 210 eV at 0.5 mm in the jet and it is lower than 50 eV after 2-mm propagation. For later times, the model overestimates the temperature because it does not take into account thermal conduction.

C. Absorption

The transmitted energy was measured using a calorimeter. This measurement gives us another opportunity to validate the model for such a regime of interaction. The energy transmission as a function of gas density is represented on Fig. 13. The full circles represent the experimental points and the empty squares represent the points calculated with the model. Figure 13 shows that at low densities ($n_e \simeq 10^{19}$ cm^{-3}) the absorption is only a few percent and it becomes greater at higher density. The relatively good agreement between theory and experiment confirms the fact that absorption comes essentially from inverse bremsstrahlung in this regime where parametric instabilities are weak.

Figure 14 shows results of a simulation demonstrating the effect of laser absorption on the pulse temporal profile. The dotted line is the initial profile and the full line is the profile after interaction with 4 mm of helium gas at $n_a=2.5\times10^{19}$ cm^{-3}. The front of the pulse is unchanged until ionization occurs. This process requires laser energy and creates a hole in the pulse profile. After ionization, laser absorption is due to inverse bremsstrahlung heating and it slowly decreases with time as the plasma is heated (this is because the absorption coefficient varies as $T_e^{-3/2}$).

IV. CONCLUSION

In conclusion, we have investigated the propagation of a randomized 600-ps laser pulse ($I=1.5\times10^{14}$ W/cm^2) in 4 mm of helium gas. Time resolved interferometry and Thomson scattering allowed us to resolve the density and temperature evolution and to retrieve density and temperature maps $n_e(z,t)$ and $T_e(z,t)$. The transmission throughout the plasma was measured and showed that laser absorption is only a few percent in the case of a gas at $n_a \simeq 10^{19}$ cm^{-3}.

A 1D model, including inverse bremsstrahlung absorption and laser diffraction, was used to fit the experimental results and showed quantitative agreement with the experiment. These results are important because they show that the delayed ionization is essentially due to beam diffraction and not to a laser absorption wave. These results also relate to ICF in the indirect drive scheme: they show the dynamics of gas ionization and plasma heating in conditions similar to those in a gas-filled cavity. Finally, this paper provides some tools to answer the question of laser propagation into a centimeter of gas for a real ICF pulse.

ACKNOWLEDGMENTS

The authors wish to acknowledge the excellent support of the laser team at LULI during the experiment. The authors would also like to thank J. P. Geindre for his very useful help in the analysis of the interferograms.

[1] D. G. Colombant and A. G. Schmitt, J. Appl. Phys. **67**, 2303 (1990).
[2] S. N. Dixit *et al.*, Appl. Opt. **32**, 2543 (1993).
[3] J. D. Lindl, Phys. Plasmas **2**, 3933 (1995).
[4] V. Malka *et al.*, Rev. Sci. Instrum. **71**, 6 (2000).
[5] J. Denavit and D. W. Phillion, Phys. Plasmas **1**, 6 (1994).
[6] H. A. Rose and D. F. Dubois, Phys. Fluids B **5**, 3337 (1993); J. Garnier, Phys. Plasmas **6**, 1601 (1999).
[7] J. Garnier, C. Gouidard, and L. Videau, Opt. Commun. **176**, 281 (2000).
[8] V. Malka, J. Faure, and F. Amiranoff, Phys. Plasmas (to be published).
[9] Y. B. Zeldovitch and Y. P. Raizer, *The Physics of Shock Wave and High-Temperature Hydrodynamic Phenomena* (Academic Press, New York, 1967).
[10] A. Y. Polishchuk and J. Meyer-Ter-Vehn, Phys. Rev. E **49**, 663 (1994).
[11] J. F. Drake *et al.*, Phys. Fluids **17**, 778 (1974).